



Pergamon

International Journal of Machine Tools & Manufacture 42 (2002) 1427–1439

INTERNATIONAL JOURNAL OF
**MACHINE TOOLS
& MANUFACTURE**
DESIGN, RESEARCH AND APPLICATION

Experimental and numerical modeling of buckling instability of laser sheet forming

Z. Hu¹, R. Kovacevic^{*}, M. Labudovic

Department of Mechanical Engineering, Southern Methodist University, PO Box 750337, Dallas, TX 75275-0335, USA

Received 30 April 2002; received in revised form 11 June 2002; accepted 13 June 2002

Abstract

New experimental results show that laser bending can be extended to generate a bending angle not only towards but also away from the laser beam, giving more flexibility to the process. In order to explain this buckling instability, a series of experiments have been carried out with real-time measurement of the bending angle for different materials, thicknesses, scanning speeds, laser beam diameters and laser powers, pre-bending conditions, and cooling conditions. Furthermore, a 3-D FEM simulation has been performed that includes a non-linear, transient, indirect coupled, thermal–structural analysis accounting for the nonlinear geometric and material properties. The buckling deformation, bending angle and distribution of stress–strain and temperature, as well as residual stresses, have been obtained from the simulations. The bending angle is affected by the temperature distribution and gradient, the mechanical and thermal properties of the sheet metal material, and the process parameters, such as the laser power, the laser beam diameter, the scanning speed, the material, the sample geometry, and other bending conditions. The buckling mechanism can be illustrated by the simulation results. © 2002 Elsevier Science Ltd. All rights reserved.

Keywords: Laser forming; Simulation; Bending; Finite element method; Instability; Buckling mechanism; Geometric nonlinearities; Material nonlinearities

1. Introduction

In addition to cutting, welding, drilling, surface treatment, and primary shaping, laser-forming is one of the new applications of the laser. Laser-forming may be used for automated production because it can be controlled very well. Experimental results show that the material can be made to bend not only towards but also away from the laser beam; in this way, laser-bending can be extended to generate concave or convex shapes; even very complex shapes can be generated. The possibility of bending the material either towards or away from the laser beam opens new ranges of applications. The recent increase in laser bending research and devel-

opment reflects the industrial interest in the process [1–6], but until now the process has been developed on the basis of empirical knowledge. Several research groups are currently investigating the fundamentals and applications, and the knowledge base is growing rapidly. Some of the physical and numerical models have been established. In the following section, three mechanisms are described that are generally considered to be the most significant in demonstrating the laser-forming behavior.

1.1. Temperature gradient mechanism

The temperature gradient mechanism (TGM) is the most widely reported laser-bending mechanism [1,7–23]. This mechanism is shown in Fig. 1. Due to the rapid heating of the surface by a laser beam and the slow heat conduction into the sheet (usually for the thick sheet), a steep thermal gradient into the material results in a differential thermal expansion through the thickness. As the material is heated, initially the thermal expansion on the heated surface (top surface) is greater than that on the cold surface (bottom surface). Counter-bending

^{*} Corresponding author. Tel.: +1-214-768-4865; fax: +1-214-768-0812.

E-mail addresses: zh26@cornell.edu (Z. Hu); kovacevi@seas.smu.edu (R. Kovacevic).

¹ Currently at The Sibley School of Mechanical and Aerospace Engineering, Cornell University, 187 Frank H. T. Rhodes Hall, Ithaca, NY 14853-3801, USA

Nomenclature

A	heat absorptivity of laser beam on sheet metal surface
c	specific heat (J/kg K)
I	thermal flux density of laser beam (J/s m ²)
k	heat conductivity (J/m s K)
\mathbf{p}	surface pressure vector (N/m ²)
P	laser beam power (J/s)
\mathbf{q}	body force vector (N/m ³)
\dot{q}	rate of heat generation (J/s m ³)
r	distance from the center of the laser beam (m)
R_1	effective laser beam radius (m)
S	area (m ²)
t	time (s)
T	temperature (K)
\dot{T}	cooling rate (K/s)
\mathbf{u}	displacement vector (m)
u, v, w	displacement components in the x, y, z directions, respectively (m)
V	volume (m ³)
Δt	incremental time (s)
ε	strain tensor in updated Lagrange configuration
ρ	density (kg/m ³)
σ	stress tensor in updated Lagrange configuration (N/m ²)
ξ, ζ, χ	local coordinates

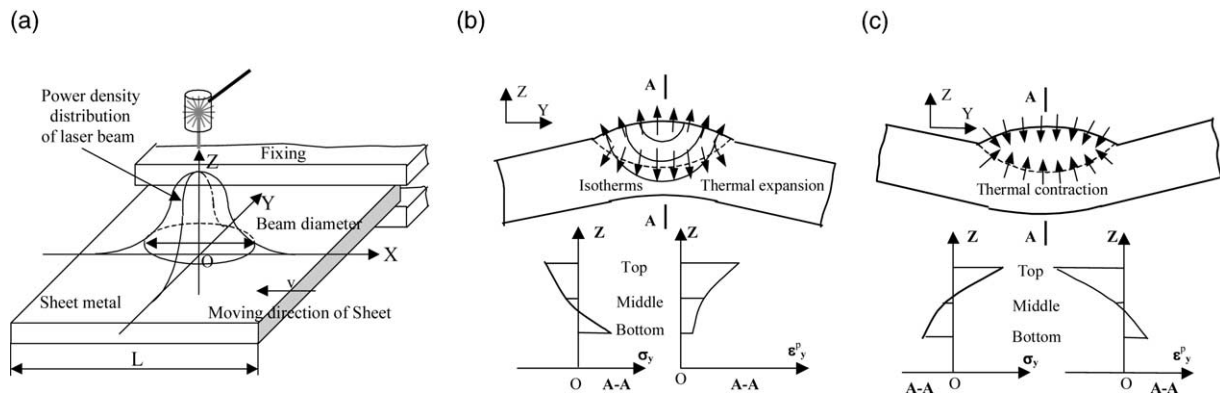


Fig. 1. Process steps of laser-bending by the temperature gradient mechanism (TGM): (a) model of laser bending; (b) heating process (counter bending); (c) cooling process (positive bending).

occurs due to the bending moment created, resulting in a small amount of plastic tensile strain at the heated surface. With continued heating the bending moment opposes the counter-bending away from the laser beam, and the mechanical properties of the material are reduced with the temperature increase. Once the thermal stress reaches the temperature-dependent flow stress, any additional thermal expansion is converted into a plastic compressive strain because free expansion is restricted by the surrounding material. During cooling the material contracts again in the upper layers, and because it has been compressed, there is a local shortening of the upper

layers of the sheet, and a bending angle develops that bends the specimen towards the laser beam.

Generally, the TGM may be used for bending thick sheets along straight lines towards the laser beam. The radiation of the surface may be repeated in order to increase the bending angle.

1.2. Buckling mechanism

If the process parameters are changed, there can be a transition to the buckling mechanism (BM) [1,7,24–27]. The BM is explained in Fig. 2. Usually in the case of

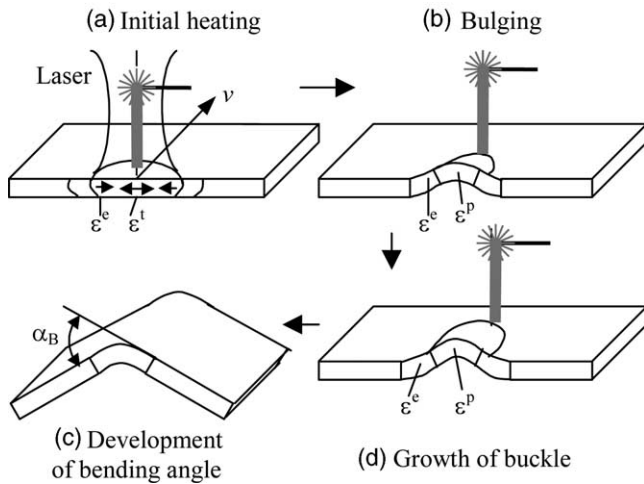


Fig. 2. Process steps of laser-bending by the buckling mechanism (BM): (a) initial heating; (b) bulging; (c) growth of buckle; (d) development of bending angle.

the BM, the laser beam diameter is much larger than the sheet thickness. The diameter of the heated area is equal to the sheet thickness for the TGM, while this diameter is ten times the sheet thickness for the BM. There is no steep temperature gradient (exactly, negligibly small compared to the gradient when working with the TGM) through the sheet thickness. The BM is activated by laser parameters that do not yield a temperature gradient in the z direction. Due to heating, thermal compressive stresses develop in the sheet which results in a large amount of thermo-elastic strain which in turn results in local thermo-elasto-plastic buckling of the material. This buckle is generated along the moving direction of the laser beam scanning. When the laser beam leaves the sheet surface, the buckle is generated across the whole sheet. The direction of the bending angle is not defined by the process itself as it is for the TGM. The part can be made to bend in either the positive or the negative z directions depending on a number of factors including the process parameters, the pre-bending orientation of the sheet, the pre-existing residual stresses, the direction in which any other elastic stresses are applied (i.e., by a forced air stream acting on the bottom of the sheet), internal stresses, and external or gravitational forces. These parameters define the direction of the buckling in a complex manner. However, it is possible to control the BM in such a way as to make it a reliable forming process.

The BM may be used for bending thin sheets along straight lines towards or away from the laser beam. It has also been suggested that BM may be used for tube forming [27]. Like the TGM, the bending angle can be increased by repeating the process.

1.3. Upsetting mechanism

The upsetting mechanism (UM) [1,7,28] is shown in Fig. 3. For the UM, the process parameters are taken in

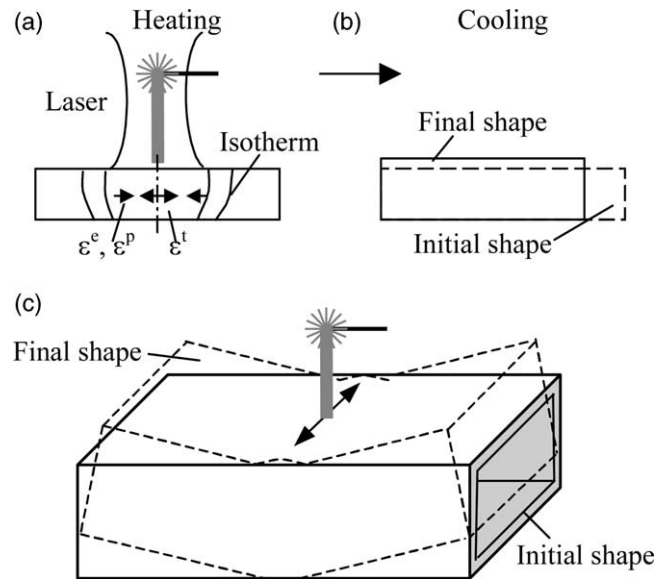


Fig. 3. Process steps of laser-bending by the upsetting mechanism (UM): (a) heating; (b) cooling.

a way similar to the BM, but the dimension of the heated area is much smaller compared to the sheet thickness. Due to nearly homogeneous heating of the sheet and the restrictions in thermal expansion from the surrounding material, the sheet is compressed with an almost constant strain along the thickness, causing a shortening of the sheet and an increase in thickness. If the sheet is heated along a line across its width, the compressive strains will remain. Repeating the process will lead to an increase in overall thickness. With the upsetting mechanism (UM), the geometry of the workpiece prevents buckling; that is to say, the thickness of the workpiece at the area irradiated by the laser beam can only thicken; it can be used to bend a pipe with various kinds of cross sections. Some of these mechanisms can accompany each other, or switch from one mechanism to another.

Though the mechanism for laser-forming is heating and cooling, Frackiewicz [29] stated that about 25 variations of such mechanisms have been investigated in the Center for Laser Technologies of Metals (CLTM) of the PASC and TU of Kielce, Poland. The parameters causing the instability were identified as the lower sheet thickness, higher heat conductivity of the material, wider beam diameter, higher laser power, and lower scanning speed. Such a combination results in a large heated area and a small temperature gradient perpendicular to the surface of the sheet. The author's new experimental results also reflect the instability in such cases. Given the complexity of analytical modeling of laser-forming processes, a numerical approach is often more beneficial for modeling these situations [1,7,14–16,20–24,26,30–36]. The improvement in computational efficiency in recent years has made such large-scale numerical studies more viable. The Boeing Company produced a finite

element model of laser-forming [14] in which two steps were adopted to simulate separately the thermal and mechanical response. The mechanical properties for structural metals at high temperatures were not available; therefore, lacking data, the properties were extrapolated. The results from the mechanical analysis were close in some cases, but in other cases were considerably less than the measured laser-forming angle data. The Massachusetts Institute of Technology (MIT), who maintained close contact with the Boeing team, produced an analytical method that was essentially the same [14,15]. MIT found similar trends in the laser-forming FEM that produced lower computed values for the laser-forming angle than the experimental results and provided useful information regarding trends on the effects of various process variables on the bending angle.

Laser sheet-forming, especially for the buckling mechanism, has features that are different from other forming processes. One feature is that the forming occurs along with large deformations such as a large deflection, large rotation, and/or large strain due to the thinness of the material and the large heating area. Another feature is the strong nonlinearity of the material and the process. Based on accurate data about the temperature-dependent mechanical properties and an accurate description of the deformation, the FEM model can predict the bend angles with a reasonable accuracy.

In order to demonstrate the unstable behavior occurring at certain parameters in the laser sheet-forming process, in this paper, the sheet metal-bending has been performed experimentally for different materials, thicknesses, scanning speeds, laser-beam diameters and laser powers, pre-bending conditions, and cooling conditions. A real-time measurement of the bending angle has been carried out. A 3-D finite element simulation has been performed that includes a non-linear transient indirect coupled thermal–structural analysis accounting for geometric nonlinearities (large deformation effects such as large deflection, large rotation and large strain) and material nonlinearities (the temperature dependency of the thermal and mechanical properties of the materials), in order to enhance the understanding of the process and thereby to increase its usage.

2. Governing equations

In order to analyze the movement and deformation of the configuration using FEM, suppose that the equilibrium states at all the time steps from time 0 to t have been obtained. The equilibrium equation at time $t + \Delta t$ can then be expressed as follows, according to the virtual work principle [37]:

$$\int_V \sigma \cdot \delta \varepsilon \cdot dV = \int_V \mathbf{q} \cdot \delta \mathbf{u} \cdot dV + \int_S \mathbf{p} \cdot \delta \mathbf{u} \cdot dS \quad (1)$$

To account for the large deformation including a large deflection, large rotation and large strain, the following shape functions for the 3-D eight-node brick element are used:

$$u = \frac{1}{8}[u_I(1-\xi)(1-\zeta)(1-\chi) + u_J(1+\xi)(1-\zeta)(1-\chi) + u_K(1+\xi)(1+\zeta)(1-\chi) + u_L(1-\xi)(1+\zeta)(1-\chi) + u_M(1-\xi)(1-\zeta)(1+\chi) + u_N(1+\xi)(1-\zeta)(1+\chi) + u_O(1+\xi)(1+\zeta)(1+\chi) + u_P(1-\xi)(1+\zeta)(1+\chi) + u_1(1-\xi^2) + u_2(1-\zeta^2) + u_3(1-\chi^2)] \quad (2)$$

$$v = \frac{1}{8}[v_I(1-\xi) \dots \text{(analogous to } u)]$$

$$w = \frac{1}{8}[w_I(1-\xi) \dots \text{(analogous to } u)]$$

where u_I ($I = I, J, K, L, M, N, O, P$) are nodal displacements

A discretization of this problem is accomplished by means of the standard finite element procedure. After aggregation, we have a group of nonlinear equations that require the Newton–Raphson method to linearize them:

$$[K]\{\Delta u\} = \{F^a\} - \{F^{nr}\} \quad (3)$$

where $[K] = \int_V [B]^T [D^{ep}] [B] dV$ is the tangential stiffness

matrix, $[B]$ is the general geometric matrix, $[D^{ep}]$ is the elasto-plastic stress–strain matrix, $\{\Delta u\}$ is the displacement incremental vector at the element nodes, $\{F^a\}$ is

the applied force vector, and $\{F^{nr}\} = \int_V [B]^T \{\sigma\} dV$ is the

Newton–Raphson restored force vector.

For the thermo-mechanical coupled system, the thermal equilibrium equation for analyzing heat transfer can be written as

$$k \left(\frac{\partial^2 T}{\partial x^2} + \frac{\partial^2 T}{\partial y^2} + \frac{\partial^2 T}{\partial z^2} \right) + \dot{q} = \rho c \dot{T} \quad (4)$$

Here, \dot{q} is mainly considered as the heat source generated by the laser beam scanning given in the form of the thermal flux density that obeys normal distribution as follows [26]:

$$I(r) = \frac{2AP_1}{\pi R_1^2} \exp\left(-\frac{2r^2}{R_1^2}\right) \quad (5)$$

To obtain the solution to the thermal equilibrium equation, boundary conditions and initial conditions are needed. The basic FEM equations for the thermal problem can be derived from the thermal equilibrium equation

$$[C]\{\dot{T}\} + [K_T]\{T\} = \{Q\} \quad (6)$$

where $[C] = \int_V \rho c [N][N]^T dV$ is the heat capacity matrix,

$[N]$ is the shape function matrix, $[K_T] = \int_V k [B][B]^T dV$

the heat conduction matrix, $\{T\}$ and $\{\dot{T}\}$ are the nodal temperature vector and nodal temperature rate vector, respectively, and $\{Q\}$ is the heat flux vector.

The basic equation for thermo-mechanical coupled calculation is as follows:

$$\begin{bmatrix} [0] & [0] \\ [0] & [C] \end{bmatrix} \begin{Bmatrix} \{\dot{u}\} \\ \{\dot{T}\} \end{Bmatrix} + \begin{bmatrix} [K] & [0] \\ [0] & [K_T] \end{bmatrix} \begin{Bmatrix} \{u\} \\ \{T\} \end{Bmatrix} = \begin{Bmatrix} \{F\} \\ \{Q\} \end{Bmatrix} \quad (7)$$

where $\{F\}$ is the force vector, including applied nodal force and the force caused by thermal strain. The indirect thermo-mechanical coupled method is used in the above equation.

3. FEM model

A computer simulation of the laser-forming process is complex. The main steps of the analysis are the thermal analysis step and the structural analysis step. In these analyses, the finite element code ANSYS was used. In order to calculate the thermo-structural coupled field with a large plastic deformation in ANSYS, an indirect coupled-field analysis (i.e., two sequential analyses) was performed. The flow chart of the FEM simulation is shown in Fig. 4. In this method, the results from the transient thermal analysis for nodal temperatures were read and applied as loads for the structural analysis. Therefore, the calculation of the temperature distribution is critical for the calculation of the stress-strain distribution. In this paper, the parameters for the thermo-

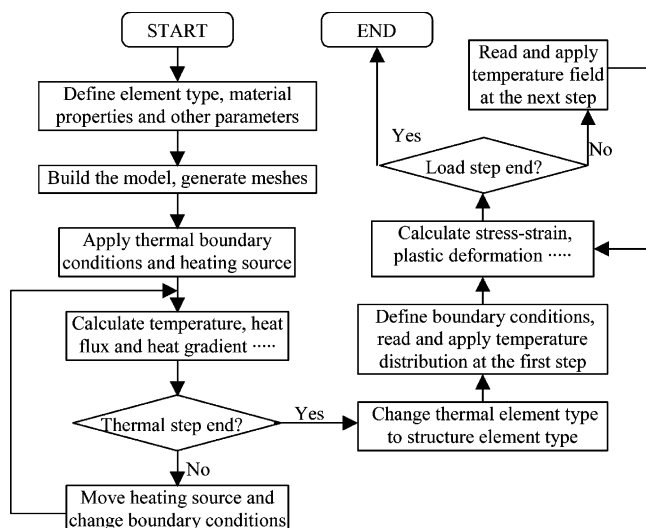


Fig. 4. Flow chart of FEM simulation.

structural calculation were obtained from Refs. [14,16,34,38,39], and the full model was calculated for the non-symmetric problem, as shown in Fig. 5. It is assumed that the sheet is flat and free of residual stresses. The elements used were the thermal analysis element SOLID70 (eight-node 3-D thermal solid with thermal conduction, and convection, and material nonlinearities) and the structure analysis element SOLID45 (eight-node 3-D solid with extra shape functions, large elasto-plastic deformation, and geometric and material nonlinearities). An ANSYS Parametric Design Language (APDL) was used to model the moving heating source according to Eq. (5). The total elements are 12,000, i.e., 40 elements along the x -direction (in length) \times 50 elements along the y -direction (in width) \times 6 elements along the z -direction (in thickness). The dimensions are 50 mm (length) \times 100 mm (width) \times 0.75 mm (thickness). In order for the steep temperature gradient to fit well, non-uniformed elements were meshed along the y -direction.

4. Experimental set-up

The experimental set-up for sheet-metal bending by laser beam scanning is shown in Fig. 6. The CW Nd-YAG laser is controlled by a computer system. The sheet metal sample was scanned forward and backward by moving the sample with respect to the stationary laser beam. The width of the samples was 50 mm, and the scanning width was 80 mm, 15 mm wider than the samples on each side. The output of the laser power and the irradiation speed were varied. Two kinds of sheet materials, carbon steel AISI 1008 and stainless steel AISI 304, were used. The experimental conditions are listed in Table 1.

The bending angle was measured on-line with an integrated machine-vision measuring system as shown in Fig. 6. The system consisted of a CCD camera (IK-M41MA) and a laser diode with a line generator. The image was acquired by using 768 (horizontal) \times 494 (vertical) pixels of a CCD camera with a focal length of 15 mm. The CCD image-plane size is 6.54 mm

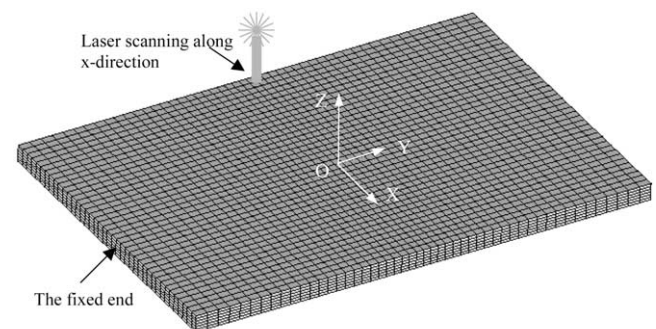


Fig. 5. FEM model.

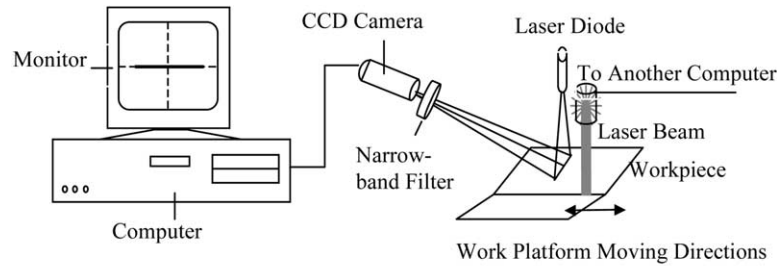


Fig. 6. Schematic configuration of the laser-bending and the bending angle measuring system.

Table 1
The experimental conditions

Materials	Size (mm ³) $L \times W \times T^a$	Laser power P (W)	Laser beam diameter d (mm)	Scanning speed v (mm/s)	Bending condition
Carbon steel AISI 1008	50×100×0.75	750	4.2	50.8	No pre-bending, and pre-bending (convex, concave)
	50×100×0.75	600	10.6	15.24, 20.32, 22.86, 24.13, 24.89, 25.40	Pre-bending (convex, concave) and no pre-bending
	50×100×0.75	500	10.0	15.24, 20.32, 30.48, 38.10	
	50×100×0.75	300	10.0, 7.0, 4.0	5.08, 7.62, 10.16, 12.70, 15.24, 17.78, 20.32,	Pre-bending (convex) and no pre- bending
	50×100×1.5	700, 500, 300	13.0, 10.0, 7.0	2.54, 3.81, 5.08, 7.62, 10.16, 15.24, 17.78	
Stainless steel AISI 304	50×100×0.75	500	7.0	12.70, 17.78, 22.86, 30.48, 38.10	
	50×100×0.75	300	7.0	7.62, 12.70, 17.78, 22.86	
	50×100×0.75	300	4.0	5.08, 7.62, 8.13, 8.51, 8.56, 8.60, 8.64, 8.89, 10.16	
	50×100×0.75	100	2.0	7.62, 12.7, 25.4	
	50×100×1.5	1000	10.0	5.08, 12.7	Without cooling, cooling at bottom, cooling at top
	50×100×1.5	750	10.0	2.54, 5.08, 10.16	

^a $L \times W \times T$ means length×width×thickness.

(horizontal)×4.89 mm (vertical). A narrow-band optical interference filter, with a central wavelength of 674 nm and FWHM of 5 nm, was used to block most of the ambient light. A frame grabber was used to deliver images to a PC with an acquisition rate of 30 frames per second. Each image was composed of eight bits of 640 (horizontal)×480 (vertical) pixels.

5. Results and discussion

Presented here is a description of all the results obtained in the experiments and the computer simulations on the buckling deformation of the laser-forming process. Every attempt is made to provide any information that could give insightful advice to potential users of the laser-forming technology.

5.1. Experimental results

In order to study the effects of the process parameters on the instability of the laser sheet-bending under the buckling mechanism, a series of experiments have been carried out. The bending angle history and the relationships between various parameters are shown in Figs. 7–11.

Fig. 7 shows the relationship between the scanning speed and the bending angle in the first scanning pass for carbon steel and stainless steel with various parameters. From the results, it can be seen that buckling deformation for stainless steel is easier and larger than for carbon steel, because stainless steel, a poor conductor of heat, can generate a higher peak temperature, which can produce higher thermal stresses to generate the buckling deformation. From the results, it can also be seen

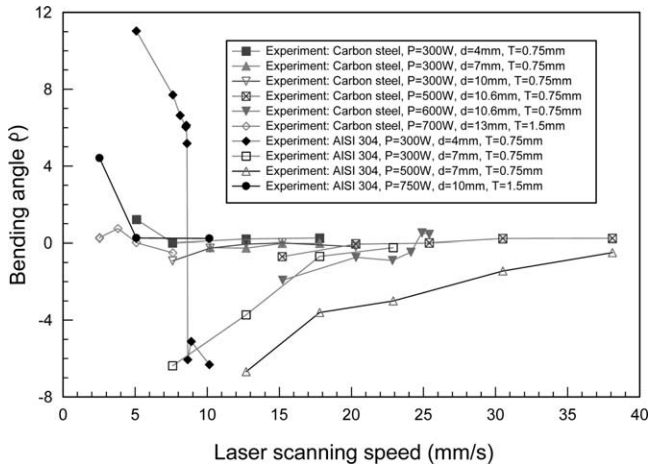


Fig. 7. Experimental relationship between scanning speeds and bending angle in the first scanning pass.

that an unstable deformation (bending convex or concave) can occur with the deformation changing from one style into another. This deformation changing is illustrated for the material AISI 304 with a power $P = 300$ W, laser diameter $d = 4$ mm, and sheet thickness $T = 0.75$ mm. In this case, when the laser scanning speed is changed from 8 to 9 mm/s, the bending angle is changed from 6 to -6° , and the deformation is changed from bending concave to bending convex due to the buckling mechanism. But in the case of the larger laser diameter, the deformation style is stable enough to bend convex. This deformation style is a very interesting phenomenon in which, under some conditions, a convex bending takes place at a higher scanning speed while concave bending takes place in the lower scanning speed. This phenomenon has not been reported in any published literature. Generally speaking, a higher heat input usually produces a larger angular distortion for the buckling deformation because the higher heat input can produce a larger temperature differential, generating greater thermal stress and buckling [24–27].

Figs. 8 and 9 show the relationship between the number of scanning passes and the bending angle with different scanning speeds for carbon steel and stainless steel, respectively. At high scanning speeds the thermal cycle is very short, which means that the heat input is very low, so the angular distortion for the buckling deformation is relatively small; while in the case of a lower travel speed, the angular distortion is much greater, as shown in Figs. 8 and 9.

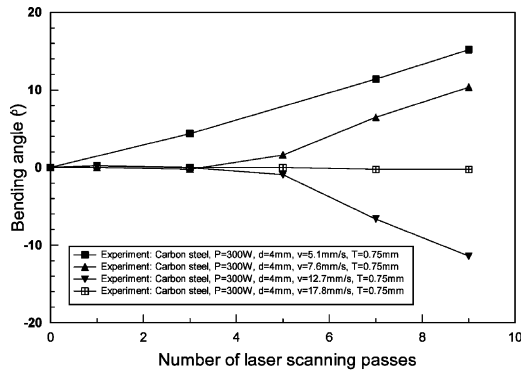
In the case of a thin plate of carbon steel and a relatively small laser diameter ($d = 4$ mm), Fig. 8(a) illustrates that as the scanning speed increases, the bending angle first decreases from positive (bending towards the laser beam) to negative (bending away from the laser beam); then, it increases to zero due to a lack of enough heat energy to generate buckling. In the case of $d = 7$ mm, see Fig. 8(b), the bending angle increases from

negative to zero as the scanning speed increases. In the case of the larger diameter, $d = 10$ mm and $P = 300$ W, see Fig. 8(c), the bending angle increases from negative to positive and then to zero due to the lack of enough heat energy for the deformation as the scanning speed increases; bending away from the laser beam easier occurs in the case of a lower scanning speed. But when laser power increases from 300 to 500 W, see Fig. 8(d), the bending angle changes from negative to zero as the scanning speed increases. When the laser power increases to 600 W, see Fig. 8(e), the bending angle increases from negative to positive as the scanning speed increases. In the case of a thick plate, see Fig. 8(f), the plate can also be bent towards the laser beam or away from the laser beam, but sometimes more than one pass is needed to set up the proper temperature distribution for buckling. In general, the absolute value of the bending angle for carbon steel can increase by repeating the process.

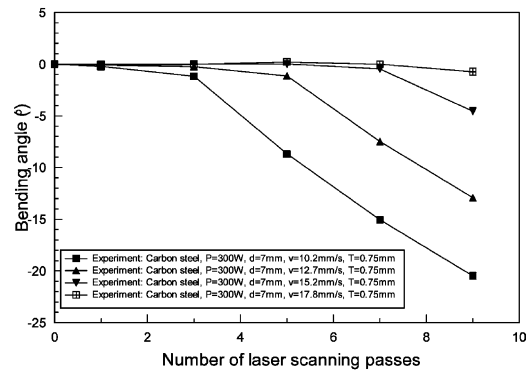
In the case of a thin plate of stainless steel and a relatively small laser diameter ($d = 2$ mm), see Fig. 9(a), the bending angle decreases from positive to zero as the scanning speed increases. In the case of $d = 4$ mm, see Fig. 9(b), the bending angle decreases from positive to negative as the scanning speed increases, and in the case of $d = 7$ mm, see Fig. 9(c) and (d), the bending angle increases from negative to zero as the scanning speed increases. However, in the case of the thick plate, see Fig. 9(e), it is difficult to bend the angle away from the laser beam. In general, the absolute value of the bending angle for stainless steel can also increase by repeating the process, and the effects of the process parameters on the bending directions for stainless steel are more complex due to its poor conduction of heat.

Fig. 10 shows the relationship between the number of scanning passes and the bending angle with the different pre-bending conditions for carbon steel. For pre-bending conditions, the materials were bent to form an angle around 10° with a bending radius of about 50 mm in order to produce a plastic deformation with residual stresses in it. It can be seen that the bending angle decreases by both convex and concave pre-bending, and the bending angle decreases much more by the convex pre-bending than by the concave pre-bending.

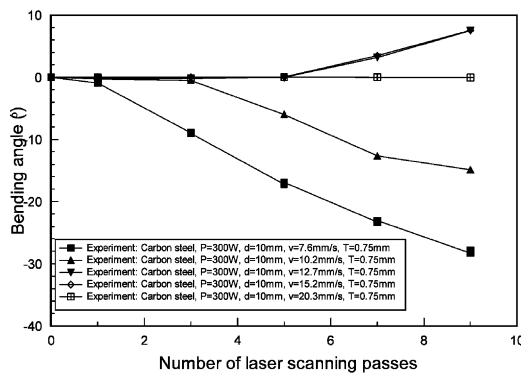
Fig. 11 shows the relationship between the number of scanning passes and the bending angle under the different conditions, including with different cooling conditions (cooling at the top surface and the bottom surface, respectively) for stainless steel, different materials (carbon steel and stainless steel), different thicknesses ($T = 0.75$ and 1.5 mm), and different laser diameters ($d = 4\sim 10$ mm). It can be seen that the strong cooling at the bottom of the thick plate can contribute to the temperature gradient mechanism so that a larger bending angle is achieved, as shown in Fig. 11(a). The bending



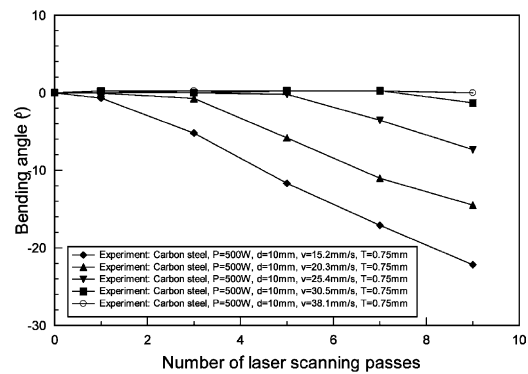
(a) P=300W, d=4mm, T=0.75mm



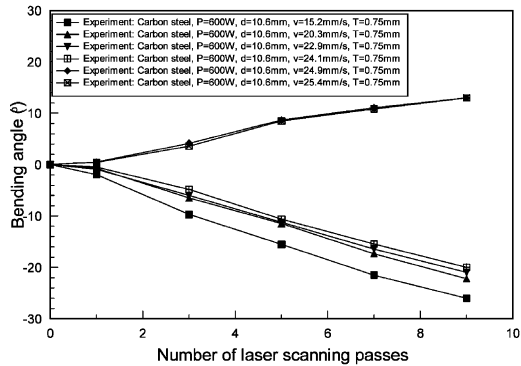
(b) P=300W, d=7mm, T=0.75mm



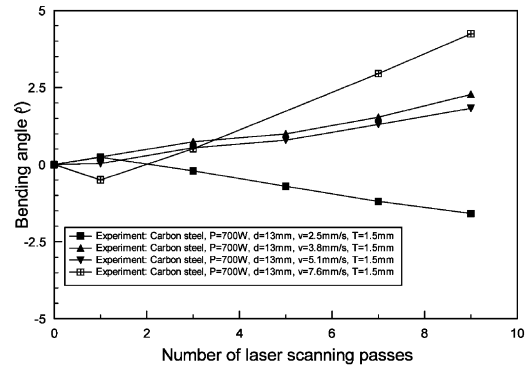
(c) P=300W, d=10mm, T=0.75mm



(d) P=500W, d=10mm, T=0.75mm



(e) P=600W, d=10.6mm, T=0.75mm



(f) P=700W, d=13mm, T=1.5mm

Fig. 8. Experimental relationship between scanning passes and bending angle with different scanning speeds for carbon steel.

deformation is quite different between the two materials with the same process parameters in most of the cases, as shown in Fig. 11(b). However, the bending angle depends on the thermal stresses produced by the temperature distribution governed by the thermo-mechanical properties and the process parameters. In the case of stainless steel, a poor conductor of heat, a higher peak temperature and temperature gradient can be generated during the heating process, so bending away from the

laser beam can occur more easily, and a larger bending angle, therefore, can be achieved in this case rather than for that of carbon steel. It can also be seen that the buckling mechanism contributes little to the thick plate in most of the cases, as shown in Fig. 11(c). In the case of different laser diameters, it also can be seen that each different laser diameter has quite a different effect on the bending angle as in the case of stainless steel, which is a poor heat conductor. But in the case of carbon steel,

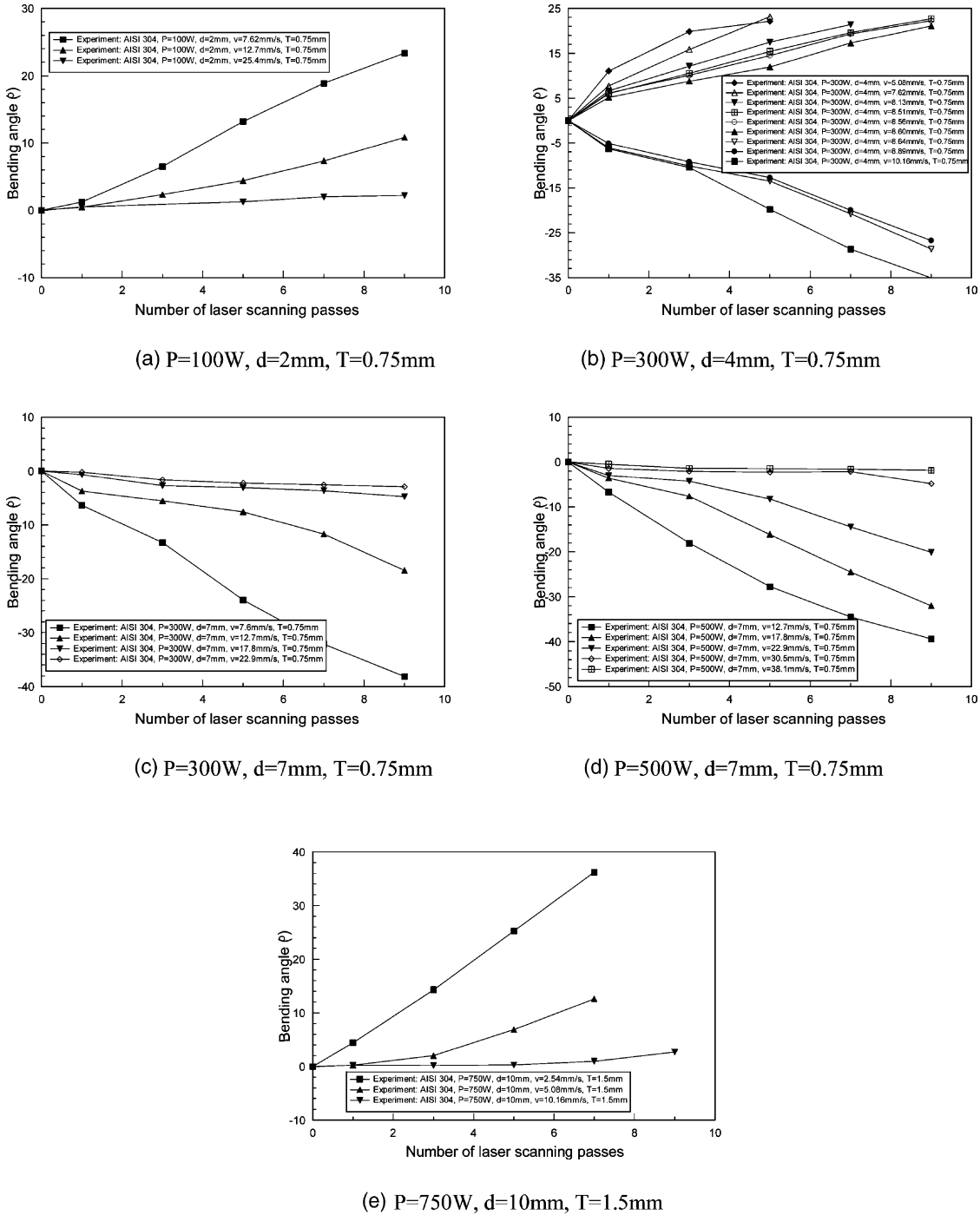


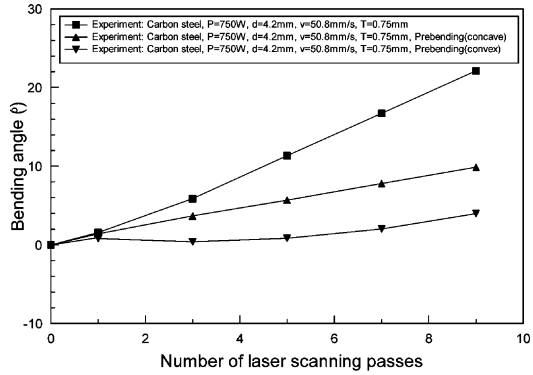
Fig. 9. Experimental relationship between scanning passes and bending angle with different scanning speeds for stainless steel.

which is a better conductor, the laser diameter has greatly affected the bending angle only after a number of passes when the temperature distribution has been set up for the buckling mechanism.

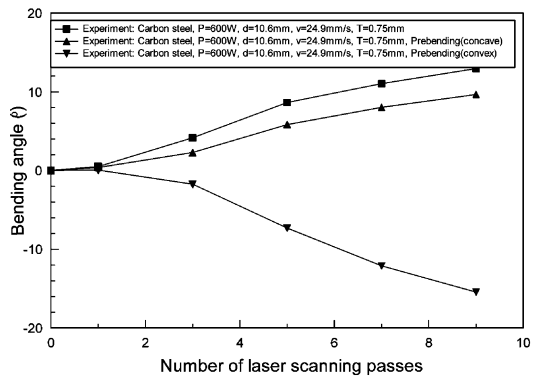
5.2. FEM analysis

Fig. 12 shows the temperature at the central points ($x = 0; y = 0; z = 0$ (top surface) and $-T$ (bottom

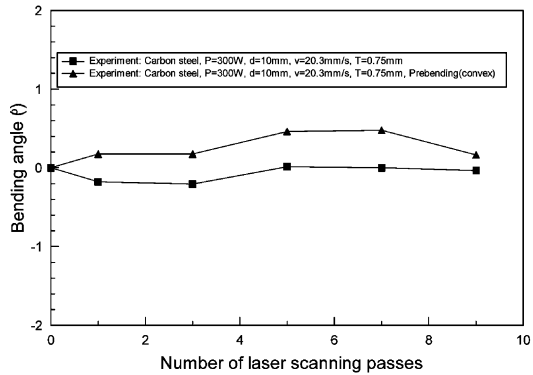
surface)) changed with the scanning time for carbon steel and stainless steel. During a laser-forming process, a typical uneven temperature distribution during a heating stage is shown in the figure for carbon steel and stainless steel. The temperature in the top surface (irradiated surface) is almost the same as, although consistently slightly higher than, that in the lower one, due to the large beam diameter, slow scanning speed, and the thinness of the sheet. The temperature gradient of the leading



(a) $P=750\text{W}$, $v=50.8\text{mm/s}$, $d=4.2\text{mm}$, $T=0.75\text{mm}$



(b) $P=600\text{W}$, $v=24.9\text{mm/s}$, $d=10.6\text{mm}$, $T=0.75\text{mm}$



(c) $P=300\text{W}$, $v=20.3\text{mm/s}$, $d=10\text{mm}$, $T=0.75\text{mm}$

Fig. 10. Experimental relationship between scanning passes and bending angle with different pre-bending conditions for carbon steel.

edge of the laser beam is steeper than that of the trail; the maximum temperature occurs in the rear of the beam, and the temperature near the heating line is higher than away from the heating line. However, the maximum temperature and temperature gradient for stainless steel are higher than those for carbon steel under the same process parameters due to the poor heat conductivity of stainless steel. It is also evident that in the case of carbon

steel, a good conductor of heat, the temperature rises slowly when it is heated and drops down rapidly when the heating source leaves it; while in the case of stainless steel, a poor conductor of heat, the temperature rises quickly when it is heated and drops down slowly when the heating source leaves it.

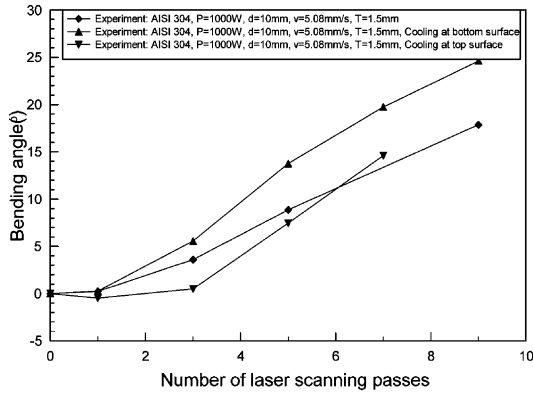
Fig. 13 shows how the plastic strain at the central points ($x = 0$; $y = 0$; $z = 0$ (top surface), $-T/2$ (middle layer) and $-T$ (bottom surface)) changes with the scanning time for carbon steel and stainless steel. Initially, the plastic strain occurs only near the heated region. The plastic region then expands to a larger region along the heating line as the heating continues and the bending angle is generated. The final deformed shape bends away from the laser beam; a residual strain can be found after cooling. As may be seen in the case where the sheet bends in a convex direction away from the laser beam, the plastic strain at the non-irradiated side of the sheet is greater and is concentrated in the region near the heating line. The plastic strain in the stainless steel is higher than that in the carbon steel; then, the bending angle for stainless steel is larger than the bending angle for carbon steel

Fig. 14 shows the comparison of the bending angles by FEM simulations with experiments. The experimental results are in agreement with the simulated ones. In the case of AISI 304, $P = 250\text{W}$, $d = 2\text{mm}$, $T = 1.5\text{mm}$ and $v = 10\text{mm/s}$, TGM plays the most important role; the bending angle is in the direction toward the laser beam under the given process parameters and the experimental conditions. The bending angle increases almost linearly with the scanning passes. In the case of $P = 300\text{W}$, $d = 2\text{mm}$, $T = 0.75\text{mm}$ and $v = 10\text{mm/s}$, BM plays the major role; the bending angle is in the direction away from the laser beam under the given process parameters and the experimental conditions. The bending angle decreases nonlinearly with the scanning passes. In this case, the experimental conditions are much more sensitive to the results due to the unstable buckling behavior.

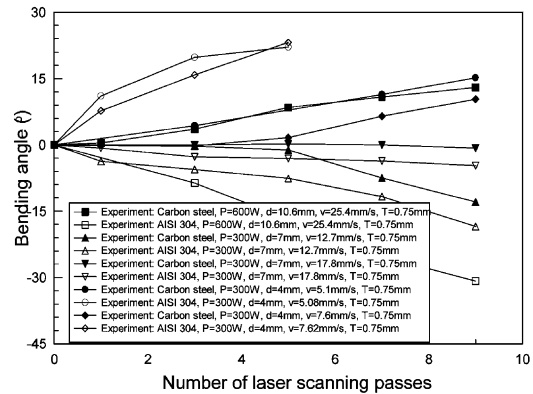
6. Conclusions

A 3-D computer simulation and an on-line experimental investigation of sheet metal-bending using laser beam scanning have been performed on the instability of the buckling mechanism. The following conclusions have been reached:

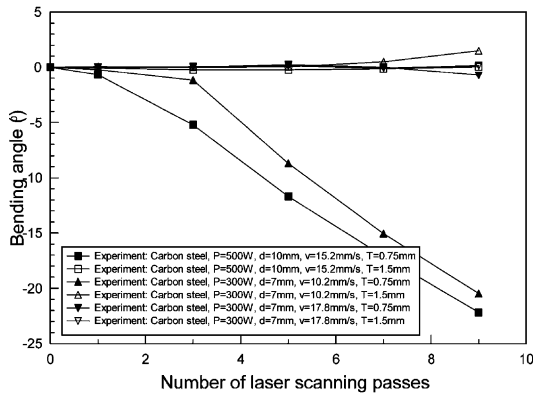
1. A 3-D FEM simulation system has been developed that includes a nonlinear transient indirect coupled thermal–structural analysis accounting for geometric and material nonlinearities. The buckling deformation, the bending angle, the distribution of stress–



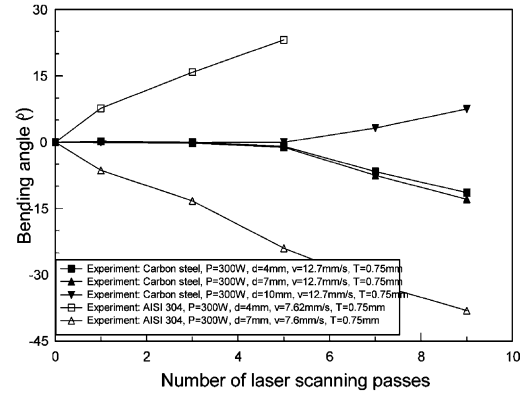
(a) with different cooling conditions



(b) with different materials



(c) with different thicknesses



(d) with different laser beam diameters

Fig. 11. Experimental relationship between scanning passes and bending angle with the different conditions.

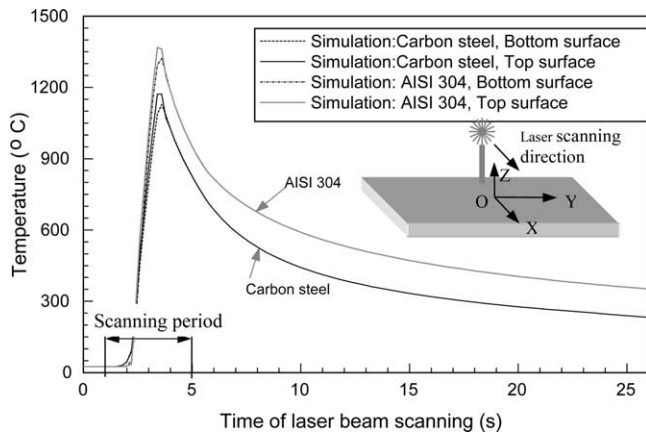


Fig. 12. Temperature distribution with scanning time at the central points [$x = 0$; $y = 0$; $z = 0$ (top surface), and $-T$ (bottom surface)] for carbon steel and stainless steel by FEM simulation ($P=300$ W, $d=10$ mm, $v=10$ mm/s and $T=0.75$ mm).

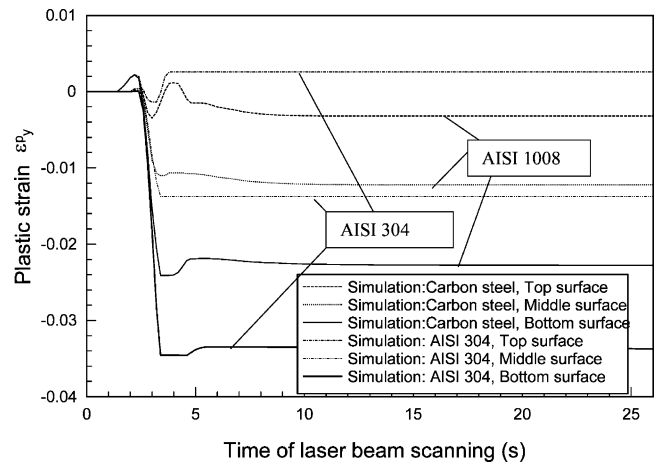


Fig. 13. Distribution of plastic strain with scanning time at the central points [$x = 0$; $y = 0$; $z = 0$ (top surface), $-T/2$ (middle layer) and $-T$ (bottom surface)] for carbon steel and stainless steel by FEM simulation ($P=300$ W, $d=10$ mm, $v=10$ mm/s and $T=0.75$ mm).

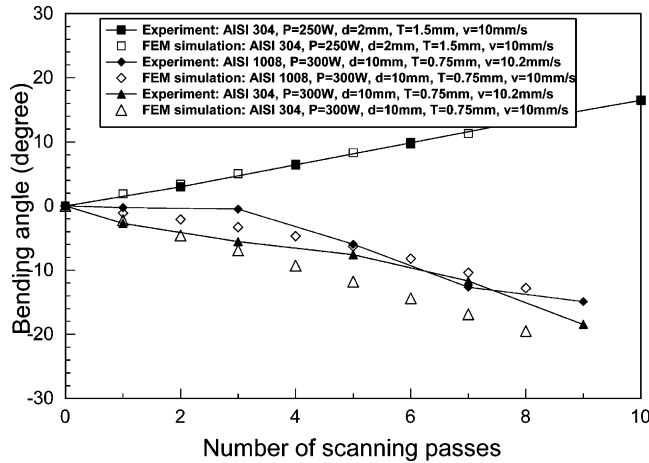


Fig. 14. Comparison of the bending angles by FEM simulations with experiments.

strain, the temperature and residual stress can all be obtained by computer simulation.

- The sheet can be made to bend in either the positive or negative z directions by a buckling deformation. The direction of the bending angle is defined by not only the process itself, but also by a number of factors such as the power, the scanning speed, and the diameter of the laser, the material and the geometry of the sheet, and the pre-bending orientation of the sheet and the cooling conditions. These parameters define the direction of the buckling in a complex manner.
- The buckling mechanism is activated by laser parameters that do not yield a temperature gradient along the direction of the sheet thickness, especially for the thin sheet, wide energy beam and the slow scanning speed. This mechanism results in a large amount of thermo-elastic strain, which in turn results in a local thermo-elasto-plastic bulging of the material starting from the edge heated first due to the thermal compressive stresses. Being continuously heated, the thermal compressive stresses develop in the sheet, and a buckle generates and develops along the heating line.
- A poorer conductor of heat, like stainless steel, a larger beam diameter and a thinner sheet thickness, a higher heat input, a lower scanning speed, and more scanning passes can more easily produce a larger buckling deformation. In this case, greater thermal stress can be achieved due to the higher peak temperature and greater temperature gradient that contribute to the buckling deformation.

Acknowledgements

This work was supported by the US Department of Education, under the GAANN Grant and NSF Grant No.EEC 9813028. Assistance by Dr H. Wang, and D.

Vasile, PhD candidate, during the experiments is gratefully acknowledged.

References

- J. Magee, K.G. Watkins, W.M. Steen, Advances in laser forming, *Journal of Laser Application* 10 (1998) 235–246.
- H. Frackiewicz, High-technology metal forming, *Industrial Laser Review*, October (1996) 15–17.
- M. Gremaud, J.D. Wagniere, A. Zryd, W. Kurz, Laser metal forming: process fundamentals, *Surface Engineering* 12 (3) (1996) 251–259.
- M. Pridham, G. Thomson, Laser forming: a force for the future?, *Materials World: the Journal of the Institute of Materials* 2 (11) (1994) 574–575.
- M. Geiger, Synergy of laser material processing and metal forming, *Annals of the CIRP* 43 (1994) 563–570.
- R.C. Crafer, P.J. Oakley, *Laser Processing in Manufacturing*, in: Chapman & Hall, 1993.
- F. Vollertsen, Mechanism and models for laser forming, in: *Laser Assisted Net Shape Engineering*, Proceedings of the LANE'94, Vol. 1, 1994, pp. 345–360.
- F. Vollertsen, An analytical model for laser bending, *Laser in Engineering* 2 (1994) 261–276.
- F. Vollertsen, M. Rodle, Model for the temperature gradient mechanism of laser bending, in: *Laser Assisted Net shape Engineering*, Proceedings of the LANE'94, Vol. 1, 1994, pp. 371–378.
- H. Frackiewicz, Laser metal forming technology, in: *Fabtech International'93*, Proceedings of the FABTECH International Conference, Illinois, 1993, pp. 733–747.
- C.L. Yau, K.C. Chan, W.B. Lee, A new analytical model for laser bending, in: M. Geiger, F. Vollertsen (Eds.), *Laser Assisted Net Shape Engineering 2*, Proceedings of the LANE'97, Vol. 2, 1997, pp. 357–366.
- Z. Mucha, J. Hoffman, W. Kalita, S. Mucha, Laser forming of thick free plates, in: M. Geiger, F. Vollertsen (Eds.), *Laser Assisted Net Shape Engineering 2*, Proceedings of the LANE'97, Vol. 2, 1997, pp. 383–392.
- M. Dovc, J. Mozina, F. Kosel, Pulse laser bending of a plate as an optodynamic process, in: M. Geiger, F. Vollertsen (Eds.), *Laser Assisted Net Shape Engineering 2*, Proceedings of the LANE'97, Vol. 2, 1997, pp. 421–430.
- Y.-C. Hsiao, H. Shimizu, L. Firth, W. Maher, K. Masubuchi, Finite element modeling of laser forming, in: *Proc. ICALEO'97*, Section A, 1997, pp. 31–40.
- Y.-C. Hsiao, Finite element analysis of laser forming, PhD thesis, Massachusetts Institute of Technology, 1997.
- K.U. Odumodu, Finite element simulation of laser shaping, PhD thesis, University of Detroit-Mercy, 1995.
- M. Geiger, F. Vollertsen, The mechanisms of laser forming, *Annals of the CIRP* 42 (1993) 301–304.
- Y. Namba, Laser forming of metals and alloys, in: *Proceedings of Laser Advanced Materials Processing, LAMP'87*, Osaka, Japan, 1987, pp. 601–606.
- Y. Namba, Laser forming in space, in: C.P. Wang (Ed.), *Proceedings of the International Conference on Lasers'85*, Osaka, Japan, 1986, pp. 403–407.
- F. Vollertsen, M. Geiger, W.M. Li, FDM- and FEM-simulation of laser forming: a comparative study, in: *Advanced Technology of Plasticity 1993*, Proceedings of the Fourth International Conference on Technology of Plasticity, 1993, pp. 1793–1798.
- N. Alberti, L. Fratini, F. Micari, Numerical simulation of the laser bending process by a coupled thermal mechanical analysis, in: *Laser Assisted Net shape Engineering*, Proceedings of the LANE'94, Vol. 1, 1994, pp. 327–336.

- [22] N. Alberti, L. Fratini, F. Micari, M. Cantello, G. Savant, Computer aid engineering of a laser assisted bending process, in: *Laser Assisted Net shape Engineering 2*, Proceedings of the LANE'97, Vol. 2, 1997, pp. 375–382.
- [23] Z. Hu, M. Labudovic, H. Wang, R. Kovacevic, Computer simulation and experimental investigation of sheet metal bending using laser beam scanning, *International Journal of Machine Tools and Manufacture* 41 (2001) 589–607.
- [24] F. Vollertsen, I. Komel, R. Kals, The laser bending of steel foils for microparts by the buckling mechanism—a model, *Modell. Simul. Mater. Sci. Eng.* 3 (1995) 107–119.
- [25] H. Arnet, F. Vollertsen, Extending laser bending for the generation of convex shapes, *Proceedings of the Institution of Mechanical Engineers Part B: Journal of Engineering Manufacture* 209 (1995) 433–442.
- [26] S. Holzer, H. Arnet, M. Geiger, Physical and numerical modeling of the buckling mechanism, in: *Laser Assisted Net shape Engineering*, Proceedings of the LANE'94, Vol. 1, 1994, pp. 379–386.
- [27] H. Frackiewicz, W. Trampczynski, W. Przetakiewicz, Shaping of tubes by laser beam, in: *ISATA 25th*, 1992, pp. 373–380.
- [28] J. Kraus, Basic processes in laser bending of extrusions using the upsetting mechanism, in: *Laser Assisted Net shape Engineering 2*, Proceedings of the LANE'97, Vol. 2, 1997, pp. 431–438.
- [29] H. Frackiewicz, Best manufacturing practices, focusing on process improvements, in: *PMA Technical Symposium Proceedings*, Vol. 3, presented at METALFORM'93, Chicago, IL, 14–17 March 1993, pp. 485–493.
- [30] A. Sprenger, F. Vollertsen, W.M. Steen, K. Watkins, Influence of strain hardening on laser bending, in: *Laser Assisted Net shape Engineering*, Proceedings of the LANE'94, Vol. 1, 1994, pp. 361–370.
- [31] T. Hennige, S. Holzer, F. Vollertsen, M. Geiger, On the working accuracy of laser bending, *Journal of Materials Processing Technology* 71 (1997) 422–432.
- [32] A.K. Kyrsanidi, T.B. Kermanidis, S.G. Pantelakis, Numerical and experimental investigation of the laser forming process, *Journal of Materials Processing Technology* 87 (1999) 281–290.
- [33] Z. Ji, S. Wu, FEM simulation of the temperature field during the laser forming of sheet metal, *Journal of Materials Processing Technology* 74 (1998) 89–95.
- [34] G. Chen, X. Xu, C.C. Poon, A.C. Tam, Experimental and 2-D numerical studies on micro-scale bending of stainless steel with pulsed laser, in: *Proceedings of the ASME Heat Transfer Division HTD-Vol. 361-4*, 1998, pp. 49–56.
- [35] T. Nakagawa, A. Makinouchi, J. Wei, T. Shimizu, Application of laser stereolithography in FE sheet-metal forming simulation, *Journal of Materials Processing Technology* 50 (1995) 318–323.
- [36] W. Li, M. Geiger, F. Vollertsen, Study on laser bending of metal sheets, *Chinese Journal of Lasers* 25 (9) (1998) 859–864.
- [37] ANSYS Theory Manual, Release 5.5, ANSYS Inc., USA, 1998.
- [38] P.D. Harvey, *Engineering Properties of Steel*, in: *American Society for Metals*, Metals Park, OH, 1982.
- [39] E.A. Brandes, G.B. Brook, *Smithells Metals Reference Book*, seventh ed., in: *Reed Educational and Professional Publishing Ltd*, 1998.